# REPORT DOCUMENTATION PAGE

AFRL-SR-AR-TR-04-
0374



**1. AGENCY USE ONLY** *(Leave blank)*

**2. REPORT DATE**

**3. REPORT TYPE AND DATES COVERED**
01 Oct 2002 - 31 Jul 2003 FINAL

**4. TITLE AND SUBTITLE**
(STTR PHASE 1) NANOPHOTONIC MODULATOR USING ELECTROMAGNETICALLY INDUCED TRANSPARENCY

**5. FUNDING NUMBERS**
65502F
STTR/TX

**6. AUTHOR(S)**
DR CHANG

**7. PERFORMING ORGANIZATION NAME(S) AND ADDRESS(ES)**
CHRONO CHROME INC
3677 JOHNSTON ROAD
BOZEMAN MT 5718-9592

**8. PERFORMING ORGANIZATION REPORT NUMBER**

**9. SPONSORING/MONITORING AGENCY NAME(S) AND ADDRESS(ES)**
AFOSR/NE
4015 WILSON BLVD
SUITE 713
ARLINGTON VA 22203

**10. SPONSORING/MONITORING AGENCY REPORT NUMBER**
F49620-03-C0002

**11. SUPPLEMENTARY NOTES**

**12a. DISTRIBUTION AVAILABILITY STATEMENT**
DISTRIBUTION STATEMENT A: Unlimited

**12b. DISTRIBUTION CODE**

**13. ABSTRACT** *(Maximum 200 words)*

This report contains three sections. The first addresses the features of Electromagnetically Induced Transparency (bEIT) and discusses particular features pertinent to this project including its associated extraordinary dispersion. The second addresses the design of resonant waveguide microring circuits to enhance the optical field inside the cavity according to the finesse, and to control the onset of ST (an nonlinear optical effect) by modulation of microring parameters - the refractive index of the ring or of the inter-ring coupling region. The third describes experimental work in which the active atomic species, praseodymium, has been introduced into the surface layer of a barium titanate crystal, an electra-optic material. Preliminary spectroscopy of praseodymium at cryogenic temperature, requisite for introducing the bEIT effects, indicates the direction of continuing work.

20040721 040

**14. SUBJECT TERMS**
NANOPHOTONIC MODULATOR AND ELECTROMAGNETICALLY TRANSPARENCY

**15. NUMBER OF PAGES**

**16. PRICE CODE**

| 17. SECURITY CLASSIFICATION OF REPORT | 18. SECURITY CLASSIFICATION OF THIS PAGE | 19. SECURITY CLASSIFICATION OF ABSTRACT | 20. LIMITATION OF ABSTRACT |
|---|---|---|---|
| Unclassified | Unclassified | Unclassified | UL |

Final Report
Nanophotonic Modulator using Electromagnetically Induced Transparency
ChronoChrome, Inc.
Alan E. Craig, Pres.
Contract F49620-03-C-0002

## Introduction and Summary

This report contains three sections. The first addresses the features of Electromagnetically Induced Transparency (EIT) and discusses particular features pertinent to this project including its associated extraordinary dispersion. The second addresses the design of resonant waveguide microring circuits to enhance the optical field inside the cavity according to the finesse, and to control the onset of EIT (an nonlinear optical effect) by modulation of microring parameters – the refractive index of the ring or of the inter-ring coupling region. The third describes experimental work in which the active atomic species, praseodymium, has been introduced into the surface layer of a barium titanate crystal, an electro-optic material. Preliminary spectroscopy of praseodymium at cryogenic temperature, requisite for introducing the EIT effects, indicates the direction of continuing work.

The major limiting realization of this work reflects the lethargy of changing coherent wavefunction superpositions in atoms. Because spontaneous relaxation mechanisms provide the mechanism for reapportionment of populations, and their efficiency is modest – requiring several cycles to achieve high transfer probability – the process is inherently slow. Particularly in identified atomic systems (e.g. praseodymium, Pr) the weak oscillator strength confers slow relaxation and narrow linewidth. Regardless of pump intensity, establishing EIT in a Pr system cannot proceed in less than 10 – 100 times the inverse of the transition linewidth using the spontaneous relaxation method for establishing coherences. This establishes a limit at around 100 Hz for modulation in this material system. Higher oscillator strength systems (e.g. semiconductor quantum dots) might circumvent this constraint to some degree; their oscillator strength is larger by a factor of 10,000,000 so presumably such a system might operate at 1 GHz or so – still a modest bandwidth in modern communication applications. Other approaches to modulating EIT are conceivable. Invoking adiabatic following can losslessly transfer population in an atomic system in about 10 Rabi periods. This approach speeds the process by about a factor of 10. Speculation that reconfiguration of the coherent population once established – without invoking spontaneous mechanisms – might occur considerably faster has not yet been fully explored.

Praseodymium doped barium titanate appears straightforward to produce. Optical waveguides have been produced previously in barium titanate by surface etching. The spectroscopy of praseodymium in this host has not yet been determined. The thin layer of doped material renders optical probing normal to the surface unproductive, so a special jig is needed to perform spectroscopy in a waveguide in a cryostat. Since only homogeneously broadened absorption lines are required to sustain EIT, the particular contributions of the host to the rare earth spectroscopy should not have critical influence.

Ring microcavities in optical waveguides present a complex array of parametric behavior. Many features of this behavior have been described in the reports on this project, apparently for the first time in any publication. In particular, tracking the propagation phase of optical fields in these resonators is critical, and is difficult using transfer matrix algebra and impossible using cascaded amplitude-dependent spectral filter approaches. The software used her to explore the characteristics of waveguide microcavities is accurate but intrinsically very slow due to the nature of the modeling approach using the finite difference time domain (FDTD) algorithm. Occasionally, the complexity of the graphical user interface impedes progress. Precision over the spatial domain and patience in the temporal domain are requisite to produce accurate and reliable results. Nevertheless, regions of the parameter space in which the optical intensity or the resonant frequency changes dramatically in response to a modest signal have been identified, in planar, two-ring, configurations. Modifications to multi-level geometries could circumvent some design problems, and extension to multi-ring (e.g. three-ring) systems could insert additional dynamics beneficially.

Collectively the realizations of this work indicate directions that remain promising. Switchable amplified optical intensity inside a waveguide microring resonator of modest finesse awaits a few more design iterations. Then the nonlinearity of the EIT response can be inserted, to enhance the sensitivity of the response to a control signal. Pending complete characterization of the spectroscopy of rare earth doped barium titanate, a device can be constructed and tested. Although praseodymium has shown EIT, resonant atoms or nanostructures (e.g. semiconductor dots) that exhibit higher oscillator strength would improve modulation bandwidth, and might circumvent the cryogenic environment needed for spectroscopy in narrow line materials.

## I. Electromagnetically Induced Transparency – Limitations and Prospects

Consider a three level atomic system. For this work we have adopted a configuration (called lambda – Λ) having two low-lying states. 'V' and cascaded configurations support similar interactions in principle. (The details related to relaxation pathways vary.) Resonant (or near resonant) excitation of one of the optical transitions with a strong coherent optical field introduces wavefunction coherence between the pair of low energy states. (In some systems, this coherence can be transferred to spins in the two energy levels; this transfer confers longer stability to the coherence.) The wavefunction coherence is generally established by a process called optical pumping, in which population from the driven transition decays spontaneously into the quiescent transition. In the presence of this coherence, absorption of a probe field on the other optical transition diminishes dramatically; this is called electromagnetically induced transparency (EIT). One way to understand this transparency is via the concept of a dark state – a non-absorbing coherent superposition of atomic wavefunctions. In EIT, the dark state is represented by:

$$|-\rangle = (\Omega_2 |a\rangle - \Omega_1 |b\rangle) / \Omega, \text{ where } \Omega^2 = \Omega_1^2 + \Omega_2^2.$$

Here $\Omega_i$ represents the magnitude of the optical field resonant with the respective transition via the expression for the Rabi frequency $\Omega = \mu \cdot 2\pi \cdot E / h$ in which $\mu$ is the transition dipole moment, E is the optical electric field amplitude, and h is Planck's constant. Analysis shows that coefficients of these magnitudes ($\Omega_2$ and $\Omega_1$) satisfy the dark state criteria; note that they incorporate the dipole moment (equivalently, oscillator strength since $f = \mu^2$), so represent atomic properties in the expression. The energy levels and photon energies of the undressed states are shown at the left in Figure 1; the bright and dark state representation appears at the right. The transition between $|-\rangle$ and $|e\rangle$ is disallowed by wavefunction interference.

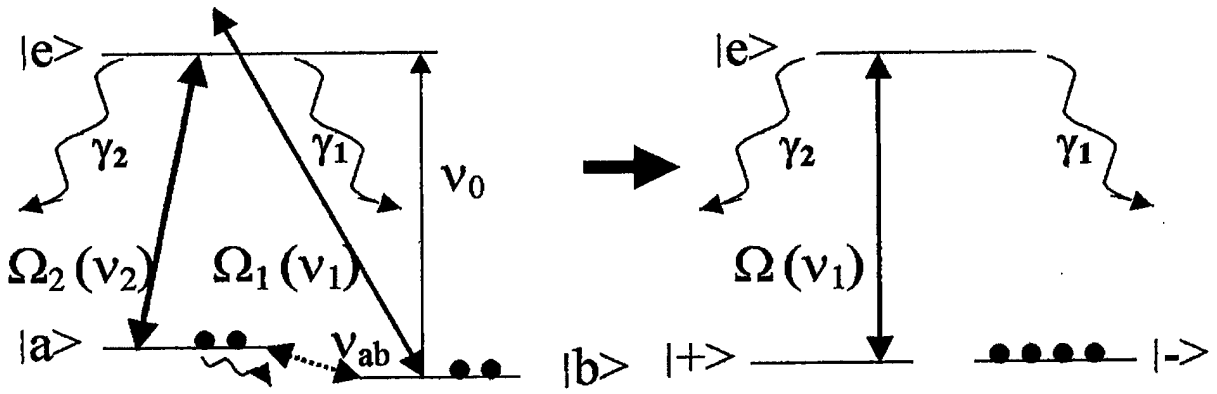


Figure 1. Atomic energy levels $|a\rangle$, $|b\rangle$, and $|-e\rangle$ and their accompanying decay constants $\gamma_i$. Coherent optical interactions are driven by the pump field at $\nu_2$ on resonance and revealed by the tuned probe field at $\nu_1$. $\nu_0$ is the resonant frequency for the probe transition. The initially balanced population of the two lower levels collects in the dark state as a result of Rabi cycling in the presence of spontaneous relaxation and phonon scattering.

A second, equivalent, view of EIT results from splitting the excited state by the AC Stark shift (or Rabi splitting). This view is illustrated in Figure 2.

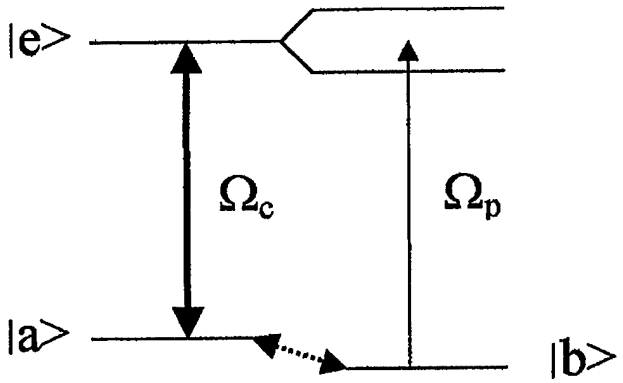


Figure 2. The pump (or coupling) field $\Omega_c$ splits the excited state by the AC Stark effect (or Rabi splitting) that results from the nonlinearity of the sinusoidal response of the excited state population to the optical driving field. The probe field then attempts to excite electrons from $|b\rangle$ into a state midway between the excited state branches. This excitation is squelched by the coherent sum of the transition probabilities.

According to either picture, EIT appears when the pump field exceeds a threshold intensity such that the associated Rabi frequency (or nutation frequency, more accurately, in a lossy system) exceeds the ground state relaxation rate $\gamma_{ab}$. In the Rabi splitting view, the splitting interrogated by the probe field must exceed the apparent linewidth of each of the two branches of the excited state. This can occur at quite small optical field amplitude, depending on the oscillator strength of the optical transition and on the ground state relaxation rate, which (surprisingly) determines the transition linewidth. (Perhaps the intuitive expectation is that the probe transition linewidth would be determined by $\gamma_1$.) This is true because phase perturbation contributions to $\gamma_1$ are common mode, so cancel out. This is particularly obvious for zero detuning of the probe. Meanwhile, spontaneous decay contributions to $\gamma_1$ remove those atoms from participation in the coherent interferometry; they no longer contribute to EIT. The width of the EIT feature is on the order of $\Omega_2$ for $\Omega_2 > \gamma_{ab}$. In our present system, based on praseodymium, $\gamma_{ab}$ is determined by spin relaxation, and is about 1/75 seconds$^{-1}$ at operating temperature (4K), negligibly small.

Accompanying this dip in the absorption is a dispersion feature, per the Kramers-Kronig relations. Since the absorption feature is a dip rather than a peak, the dispersion is normal rather than anomalous in character. In fact, the dispersion is extraordinarily steep, albeit over a very narrow linewidth. Pictures of modeled EIT features appear in Figure 3. Either the absorption dip or the dispersion might be exploited in a device, with the caveat that the full apparent frequency range for the extraordinary dispersion is limited by absorption at either end. Slow light propagation depends on this extraordinary dispersion, specifically on the slope of $\chi'(\omega)$; this is a *group* velocity. The excursion of the *phase*

velocity or, equivalently, the range of the refractive index over the bandwidth of the extraordinary dispersion (that is, over $\Delta\omega = \Omega_2$) can be calculated with care to be a very modest number: $\Delta n \approx 6 \times 10^{-4}$ for the experiment published by Hemmer et al. based on praseodymium. * This number is nearly independent of material constants for an optical density of 1. A fundamental (Fourier) constraint of slow light propagation limits the number of consecutive pulses simultaneously within the medium to only one. A shorter pulse means higher bandwidth. To obtain higher transparency bandwidth entails sacrificing the slope of the dispersion (by Kramers-Kronig), so the pulse speeds up.

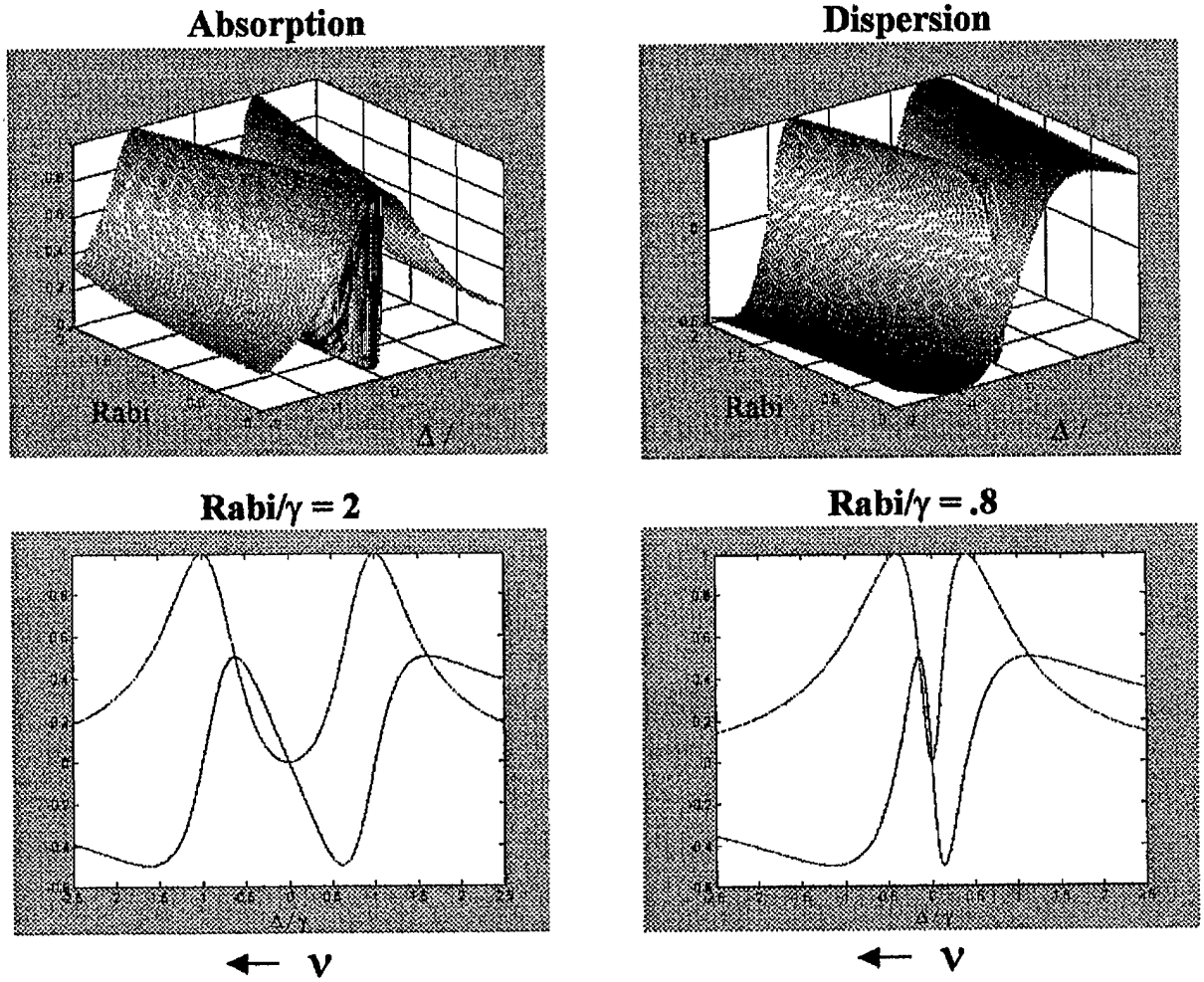


Figure 3. Top two graphs: Absorption and Dispersion dependence on the Rabi frequency (conferred by the optical pump field) as a function of the detuning $\Delta$ of the probe field from resonance. (The normalization denominator $\gamma_{ab}$ for both Rabi and $\Delta$ failed to appear after transferring the graphs from Powerpoint.) Bottom two graphs: selected cross sections along the detuning axis for two values of the Rabi frequency. Note: the convention for positive detuning corresponds to smaller probe field frequency.

* This value for $\Delta n$ can be calculated as follows: The Hemmer slow light result recorded a group velocity of 33 m/sec using a probe pulse having 100 KHZ bandwidth to reveal a transparency window 70 KHz wide. $v_g = d\omega/dk = 33$ m/sec, so $dk = d\omega/v_g = 133$

$cm^{-1} = k_0 \Delta n$. Thus $\Delta n = 6.35 \times 10^{-4}$. Other systems with higher oscillator strength will exhibit different absolute numbers, but they are all surprisingly small because of the exceedingly narrow transparency window.

The time required to establish EIT in general depends on $\gamma_1$, since it is via this relaxation that electrons escape the Rabi oscillations on the $|a\rangle - |e\rangle$ transition and appear in the dark state. Electrons that relax spontaneously or by scattering can reappear in the bright state (on average, half the time, given similar pathways and selection rules) so becoming 99% dressed requires at least a time of about $7 \times \gamma_1^{-1}$ ($2^{-7} = 1 / 128$), discounting the time to initiate population into the excited state by the optical pump field. Depending on the strength of the pump, the excitation time can be appreciable, but in any case must exceed the reciprocal of the linewidth of the homogeneously broadened optical transition – the feature completely saturates at higher optical pump power. This means that EIT is slow to establish (by this means). As an example, for $\gamma_1 \approx 100$ μsec as in praseodymium the turn-on time might exceed several milliseconds.

An alternative approach to initiating EIT can be faster. It has been espoused by Phil Hemmer (Texas A&M University, Department of Electrical Engineering) but perhaps not yet tried experimentally in establishing EIT. The approach introduces adiabatic transfer of the atomic population between energy levels. It uses two resonant pulses, tuned to the two optical transitions, in a counter-intuitive sequence to transfer electrons from one low lying level to the other. It can accomplish this process in approximately time $T = 10 / \Omega_2$ without actually populating the excited state. This time can be considerably shorter than that achieved relying on relaxation mechanisms included in $\gamma_1$. A cogent derivation and explanation of this phenomenon can be read in a landmark paper (Ref 1) from which the following figure is borrowed:

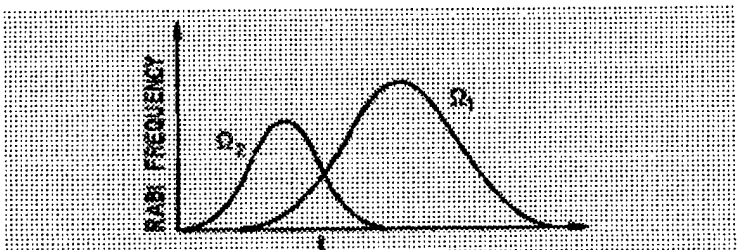


FIG. 2. Time dependence of the Rabi frequencies required for efficient population transfer under adiabatic following conditions.

Figure 4. Visualization of the two-pulse counterintuitive pulse sequence that produces adiabatic population transfer. The population is originally resident in level 1 (corresponding to $|a\rangle$ in the preceding discussion).

EIT exhibits a second shortcoming, at least in homogeneously broadened media. The narrow-linewidth transparency feature indicates that only probe pulses having narrow bandwidth can propagate as slow light. Higher frequency spectral components overlap the range of high absorption in the wings of the EIT absorption dip. Attempts to broaden the spectral linewidth of the EIT feature by increasing the Rabi frequency introduced by the pump field flatten the dispersion and obviate the slow light mechanism.

Regardless of the oscillator strength, this observation holds for all dense media (optical density greater than 1.)

## II. Optical Waveguide MicroRing Resonators

We have continued to improve the waveguide micro cavity modeling and to ferret out the inconsistencies and misconceptions in layout. A new computer with 2.8 GHz clock and 1 GByte of DRAM was purchased to expedite modeling, resulting in apparent speed up exceeding a factor of 4. (Even for these straightforward waveguide circuits, the RSoft FDTD package runs exceedingly slowly, requiring several hours to complete the propagation of the field through the structure at optimal grid resolution.) A new adaptation of the two-ring scheme, shown in Figure 5 (below), was constructed. The layout minimizes lateral extent, to speed the FDTD computation, while simultaneously balancing the propagation delay in the two insertion branches of the bus waveguide. This layout yielded several realizations that will be reviewed below.

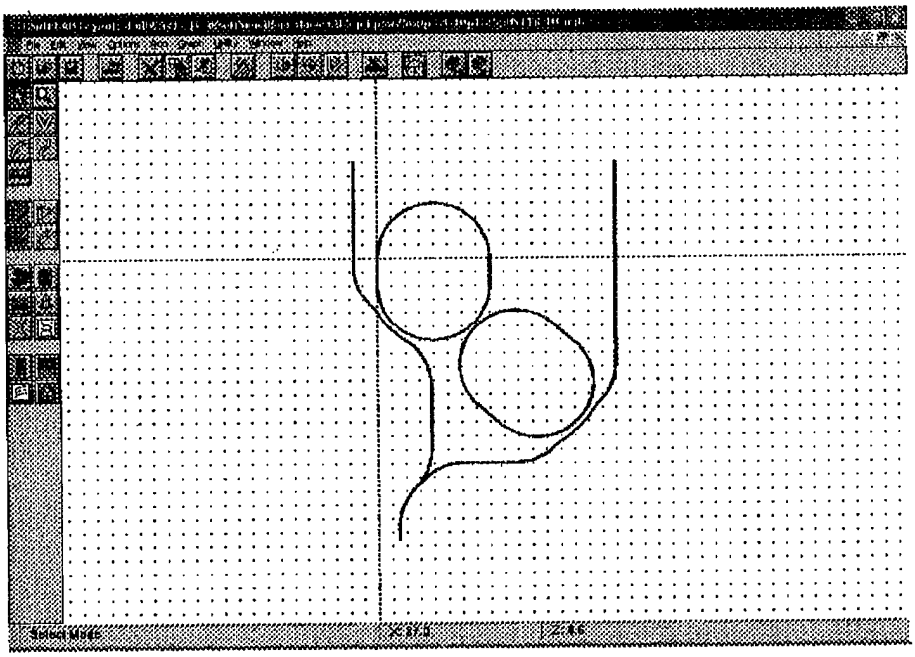

Figure 5. This two-ring layout exhibits only a short section in the left-hand ring where the pump intensity will differ. The ovals have been shortened for faster computation. The path lengths from common launch to the bus-to-ring coupling points are identical unless the right-hand ring is rotated using a layout parameter.

This configuration was also modeled in Excel to learn the dependence of the optical intensity at an arbitrarily chosen point in the left hand ring on the relative refractive indices of the two rings and on their angular offset. (This angular offset, in

practice, could be fixed by patterning or, equivalently, replaced by modifying the phase of the light injected from the bus.)

- The k-vector of the light (and consequently the detuning of the cavity) is a sensitive control parameter for internal optical intensity in the waveguide ring. This is no surprise; a single ring with high finesse shows a narrow transmission peak (and concomitant internal intensity peak) corresponding to the cavity filter response.
- Likewise, introducing a difference in refractive index in the two ring waveguides quickly spoiled the joint finesse. This effect is periodic (although not sinusoidal) in the index difference, with periodicity corresponding to the free spectral range of the microring cavities. Simply, tuning the effective cavity length changes its resonant frequencies.
- Note that for any resonance feature, the accompanying dispersion varies by nearly $2\pi$ over the FWFM excursion of the absorption feature. Thus the interferometric phase detuning occurs over the same narrow frequency range as the amplitude transmission passband.
- The internal intensity varies as a sinusoidal function of the angular offset. The angular offset modifies the phase of the light injected into the right hand ring. The path from injection into the bus to the ring lengthens, and the path around the ring to the ring-to-ring coupling point shortens. These effects counter each other, but the location of the center of rotation prevents their canceling entirely. The periodic dependence of intensity on angular offset might be expected to equal $2\pi/m$, where m is the number of optical wavelengths around the periphery; the partial compensation contributed by propagation in the bus increases this number considerably.

Modeling with the FDTD program produced the following observations.

- Changing the gap widths revealed the appropriate ring-to-ring and bus-to-ring spacing for low transmission (and high effective reflectivity), and concomitant high finesse. The optimal settings depend on the waveguide width, since a narrower waveguide provides weaker optical field guiding and confers more extended evanescent field tails. For weak confinement, radiation losses at bends are bothersome, and coupling between waveguide structures occurs in unexpected regions. Using a waveguide refractive index of 1.8 confers a maximum waveguide width of about 200 nm for single mode waveguiding. If the refractive index is 2.4 instead, the maximum single-mode width decreases to 68 nm.
- In the case of modest coupling, long coupler interaction lengths support undesirable oscillation in the optical power transfer. Optical power couples first into the ring from the bus, then back out as the internal field grows to exceed that in the bus. The wide gaps needed for high finesse are less susceptible to this effect. Monitoring the optical intensity coupled from bus to ring at small intervals throughout the coupling region revealed that this effect is noticeable but not severe for a waveguide width of 150 nm and a bus-to-ring gap of 200 nm. Setting the gap at 320 nm in a later simulation (where the waveguide width was only 90 nm) showed bus-to-ring coupling of about 5%, which is still modestly larger than optimal to allow high optical intensity internal to the rings. The apparent reflectivity of the coupling region needs to exceed about 95% before the internal optical intensity exceeds the bus optical intensity; that is, the finesse exceeds unity. Discussion of this criterion will be expanded in a later paragraph.

- An optimal waveguide width can be discovered for determining the extent of the evanescent fields across the coupling gaps. Too wide a waveguide produces short evanescent tails that couple only across very narrow gaps; too narrow a waveguide produces excessively long tails that extend through and beyond the recipient waveguide.
- In the region of waveguide coupling, the value of the effective longitudinal propagation constant $\beta$ decreases. The propagating field overlaps the neighboring waveguide, thereby occupying two high index regions simultaneously; it slows down. This changes the resonant conditions for each microring, since the cavity optical path length increases. This effect has dramatic ramifications for coupled two-ring geometries, as will be explained below.

The FDTD program produces a plot of the optical amplitude vs. frequency at each of the intensity monitors inserted into the waveguide path. From the obvious resonances, the free spectral range of the rings can be calculated, and from it the number of optical wavelengths around the ring perimeter. This calculation must be approached with care. Generalized dispersion curves can be computed that show the relation of $\beta$ (and hence the plane wave propagation angle inside the waveguide) to the waveguide width. These curves appear, for example, on page 24 of Tamir's book "Integrated Optics" in the chapter written by Kogelnik (Reference 3). Starting with the assumption that the waveguide is near maximum width to support only the fundamental transverse mode, the propagation angle can be calculated by inspection of the dispersion curves. Based on this angle, $\beta$ can be calculated, since $\beta = k_0 \, n \sin(\theta)$. Then the mode number (corresponding to the number of optical periods around the perimeter of the rings) is approximated by $m = P \cdot \beta / (2\pi)$. Since $\beta$ is not constant in the coupling region, modest extra optical path length is accumulated there that is not reflected in this formula. Knowing m aids in estimating the adjustment in the angular orientation of the right ring that will dephase the light that it provides to the left ring with respect to the light occupying the left ring as a result of coupling from the bus. The mode number calculation performed in this manner produces a dramatically different result from that obtained by dividing the perimeter (P) by the wavelength. This result is due to the impact of the Goos-Hanchen Effect. Since absorption and finite path render the model of reciprocating plane wave propagation within the waveguide a fiction, the spatial dispersion in the phase delay on reflection from the total internal reflection boundaries must be accommodated. This accommodation is known as the Goos-Hanchen Effect, after its discoverers. The import is that considerably more phase accumulates as the optical field propagates down the waveguide than would by clean reflection at the material boundaries – as if the waveguide were nearly three times as wide.

Based on the expressions for a Fabry-Perot etalon resonator (two plane parallel reflectors), an expression was derived that represents the optical intensity (Ix) inside a microcavity ring resonator.

$$I_x = I_0 \, t_1^2 / (1 + r_1^2 \, r_2^2 - 2 \, r_1 \, r_2 \cos(\delta)$$

In this expression, $r_1$ is the optical amplitude in the bus downstream from the coupling region to the microring; it corresponds to a reflectivity. Likewise, $t_1$ is the optical amplitude transmitted from bus to ring. Similarly, $r_2$ is the optical amplitude retained in

the ring after the light passes by the outcoupling region, to the second bus, on the opposite side of the microring. $I_0$ is the optical intensity in the input bus waveguide. The angle $\delta$ is the round trip optical path length. On resonance $\delta$ is an integral multiple of $2\pi$ so that the cosine factor is unity, the sole case that we will consider.

In a double ring configuration the field in the left ring is the sum of the light entering from the left bus and that entering from the right ring. Solving for the internal intensity from each vantage, taking the square root to obtain the field amplitude, then summing the two field contributions with an adjustable phase and squaring the result will yield the possible intensity range in the left ring for any configuration. A caveat pertains: here we consider each ring resonant with the incident light frequency, and a symmetric geometry so that the bus-to-ring coupling is the same on both sides. (The ring-to-ring coupling can differ.) This obviates the requirement to track the relative phase of the light in each ring. As we will see below, the phase contributions introduced by the coupling regions renders maintaining this condition problematical.

An expression for the effective reflectance of the left ring from the vantage of the right ring can be derived, bearing in mind that the left ring also has backside transmission into the left bus. This expression is

$$R = \{r_1^2 + r_2^2 - 2\, r_1\, r_2 \cos(\delta)\} / \{1 + r_1^2\, r_2^2 - 2\, r_1\, r_2 \cos(\delta)\}$$

where $r_1$ is the ring-to-ring reflectivity and $r_2$ is the ring-to-bus reflectivity.

The transmittance expression at the same point is

$$T = t_1^2\, t_2^2 / \{1 + r_1^2\, r_2^2 - 2\, r_1\, r_2 \cos(\delta)\}$$

where $t_1$ is the ring-to-ring transmissivity and $t_2$ is the ring-to-bus transmissivity.

Note that while $R + T = 1$ by conservation of energy, $r^2 = R$ and $t^2 = T$, but $r + t$ is not necessarily equal to unity because of the phase properties of the coupling. (In a plane mirror dielectric resonator, usually $r - t = 1$.) Figure 6 plots the reflectance R vs. $r_1$ for several values of $r_2$. Large values of R occur only for $r_1$ near unity, and only when $r_1 > r_2$. The next section reveals that large R is required to obtain large intensity in the left ring.

Retrieving the expression for the internal intensity from a preceding paragraph, and substituting R for $r_1^2$ and T for $t_1^2$ gives

$$I_x = I_0\, T / (1 + R\, r_2^2 - 2\, \sqrt{R}\, r_2 \cos(\delta).$$

This expression is plotted in Figure 7. To obtain sensitive dependence on the parameters of the rings (refractive index, or effective coupling gap, e.g.) operation must occur at

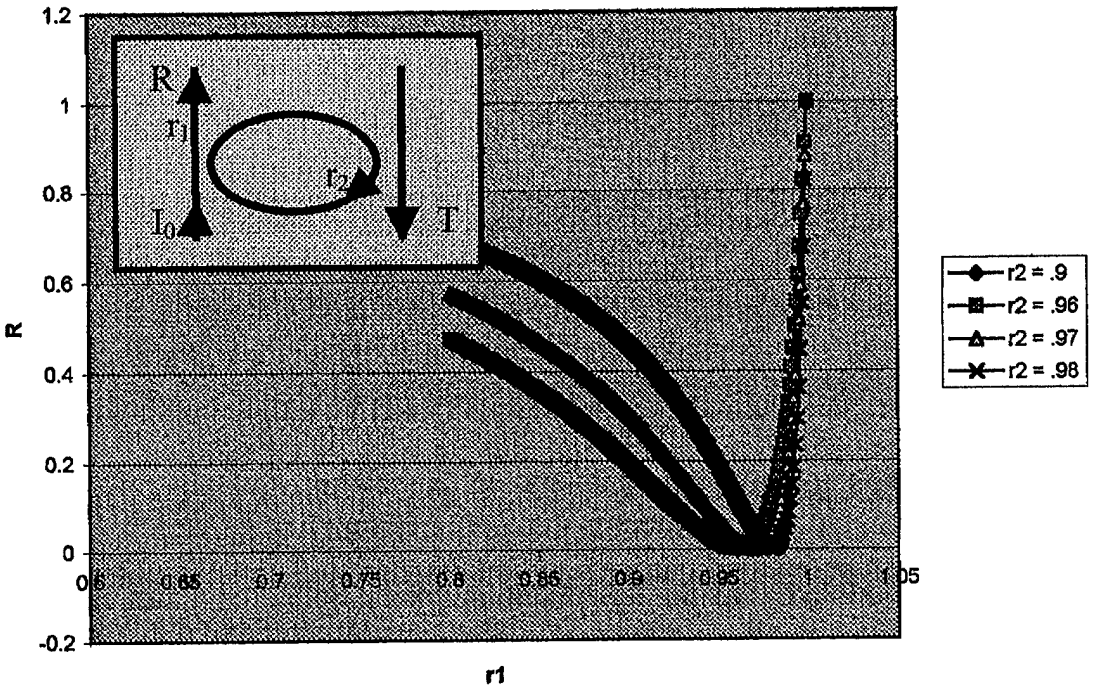


Figure 6. The reflectance of a single ring resonator, between two coupling ports, into the insertion coupler. See inset.

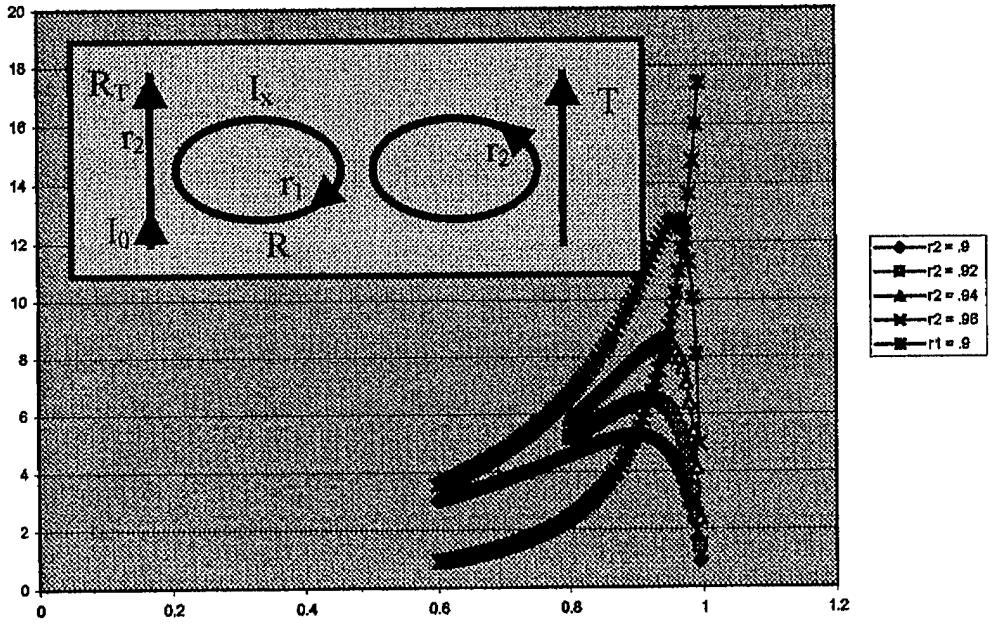


Figure 7. Intensity in left ring as a function of bus-to-ring reflectivity (humped curves). Rising curve abscissa is ring-to-ring reflectivity – the ordinate of Figure 6.

high reflectivity, at the far right of Figure 7, where the curves are steep. This region requires weak coupling between rings and buses, and between the two rings. So the gaps should be wide. This indicates high intrinsic finesse in the rings. Care to avoid limitations imposed by radiative or absorptive losses would be important in practice.

Coupling between the microrings in the two-ring configuration perturbs the resonance spectra. In simulation, the bus waveguides were removed and the optical field was launched within the rings, first for each ring separately, then for the two rings coupled. Although the geometry is symmetric and the rings' perimeters are identical in length, the spectrum of the coupled rings exhibits two sets of peaks, as shown in Figure 8. Each set has the same inter-peak spacing (the same free spectral range). The left peak in each pair in the figure is shifted to slightly lower frequency while the right peak moves to higher frequency by about three times as much. Evidently, two trajectories for optical fields exist. The first trajectory circulates only in one ring. The addition of the coupling region slows propagation in that region and (to first order) lengthens the wavelength required for resonance, or reduces the frequency. The second trajectory executes a figure eight between the two rings. Apparently, cross-coupling effectively speeds up optical propagation, although the mechanism for this acceleration is unclear. Perhaps the retardation is increased compared to the single ring case! Careful analysis of the spectra could reveal the order number of each peak. Smaller rings would increase the free spectral range (FSR) and decrease the mode numbers, revealing the difference in FSR between the two sets of spectral peaks. The surprise here is that not only is coupling efficiency non-reciprocal in the curvature of coupled waveguides, but phase accumulation in the coupling region for reflectance differs from that for transmission. Whether this observation leads to a sensitive control mechanism for modulation or serves only as a nuisance for design and fabrication remains to be learned.

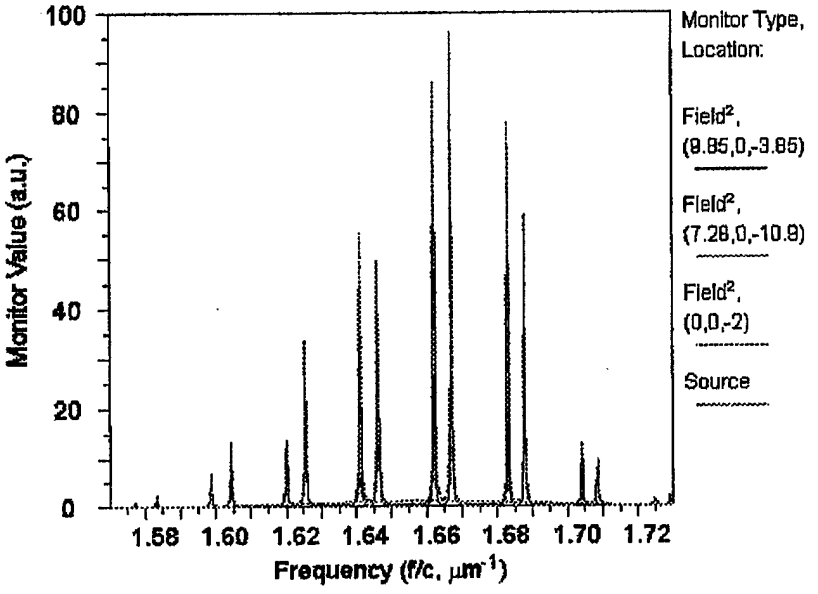


Figure 8. Coupled microrings show two sets of spectra, one for a single-ring trajectory, the other for a figure eight trajectory.

III. EIT Materials: Praseodymium in Barium Titanate

The following report was written by collaborator David Towner working in the laboratory of Bruce Wessels at Northwestern University. Figures and references are numbered independent of those elsewhere in this report.

Pr-doped barium titanate thin films by MOCVD

Barium titanate ($BaTiO_3$) thin films doped with praseodymium have potential as a powerful electro-optically active medium which can also undergo electromagnetically induced transparency (EIT). The large solubility of rare earth dopants in barium titanate allows higher dopant densities than in most glassy materials. High quality thin films of barium titanate have been grown by metal-organic chemical vapor deposition [1], and can be formed into low loss optical waveguides (<1 dB/cm). Such films allow formation of waveguide-based photonic devices, such as modulators and resonators.

In Phase I of this STTR, we report the first successful growth of Pr-doped $BaTiO_3$ thin films. An MOCVD process was specifically developed for this dopant system, and phase pure Pr:$BaTiO_3$ films grown. X-ray and m-line spectroscopy analysis show the films are of excellent quality.

**Background:** For EIT applications, Pr should be incorporated in the $BaTiO_3$ lattice in the 3+ oxidation state, making it a donor on the Ba site or an acceptor on the Ti site. Substitutional site preference depends on several factors, including ionic radii size, valence, stoichiometry (Ba or Ti-rich), oxygen partial pressure, and temperature. Incorporation of rare earth dopants in $BaTiO_3$ has been studied both theoretically [2] and using bulk ceramic techniques [3]. For the case of Pr3+, substitution most readily occurs on the Ba site. However, at elevated temperatures and high oxygen partial pressures, incorporation of Pr4+ on the Ti site can occur isovalently, with the dopant reducing to Pr3+ upon cooling.

**Results:** $BaTiO_3$ thin films were epitaxially grown on MgO (100) substrates using a horizontal MOCVD reactor [1] equipped with a quartz boat to hold the dopant precursor, ($Pr[THD]_3$). For these initial films, the substitutional chemistry was controlled by intentionally skewing the growth conditions to favor incorporation of Pr3+ as a donor on the Ba-site. This was done by setting the stoichiometric $BaTiO_3$ growth conditions to be roughly 1% Ti-rich, then adding increasing amounts of Pr until a phase pure film was formed. By this methodology, the final film should be roughly 1% Pr3+, all on the Ba site.

The crystalline structure of the Pr-doped $BaTiO_3$ thin films was studied using high resolution x-ray diffraction. The only peaks observed in the theta-2theta scans belonged to the $BaTiO_3$ (001/100) family of peaks and the MgO substrate (Figure 1), indicating epitaxy between film and substrate and the absence of any impurity phases. The films were polydomain (polarization both in and out of the plane of the film), as indicated by the peak-splitting of the 002/200 peak in Figure 2. No significant shifts in the peaks' positions were observed. The crystalline quality of the film was evaluated using the rocking curve of the $BaTiO_3$ (200) peak, with a full width at half maximum (FWHM) of 0.32 (Figure 3). This is comparable to the best undoped $BaTiO_3$ films on MgO (FWHM=0.28), and indicates a high degree of crystalline perfection.

A Pr-doped $BaTiO_3$ thin film of thickness suitable for optical waveguiding was evaluated using the method of m-line spectroscopy, whereby a rutile prism is used to

stimulated optical guiding modes in the planar waveguide. Measurements were performed at a wavelength of 632.8 nm. As shown in Figures 4 and 5, the Pr-doped $BaTiO_3$ planar waveguide supported two modes in both the transverse electric (TE) and transverse magnetic (TM) polarizations. The film thickness and refractive indices were determined from the positions of the modes, giving $n_{TE}$= 2.356, $n_{TM}$= 2.368, and t=471 nm. The birefringence, $\Delta n$=0.012, is lowered by the polydomain structure of the film.

**References**

[1] D.J. Towner, J. Ni, T.J. Marks, and B.W. Wessels, *J. Cryst. Growth* **255** (2003) 107.
[2] M.T. Buscaglia, V. Buscaglia, and M. Viviani, *J. Am. Cer. Soc.*, **84** (2001) 376.
[3] Y. Tsur, T.D. Dunbar, and C.A. Randall, *J. Electroceramics*, 7 (2001) 25.

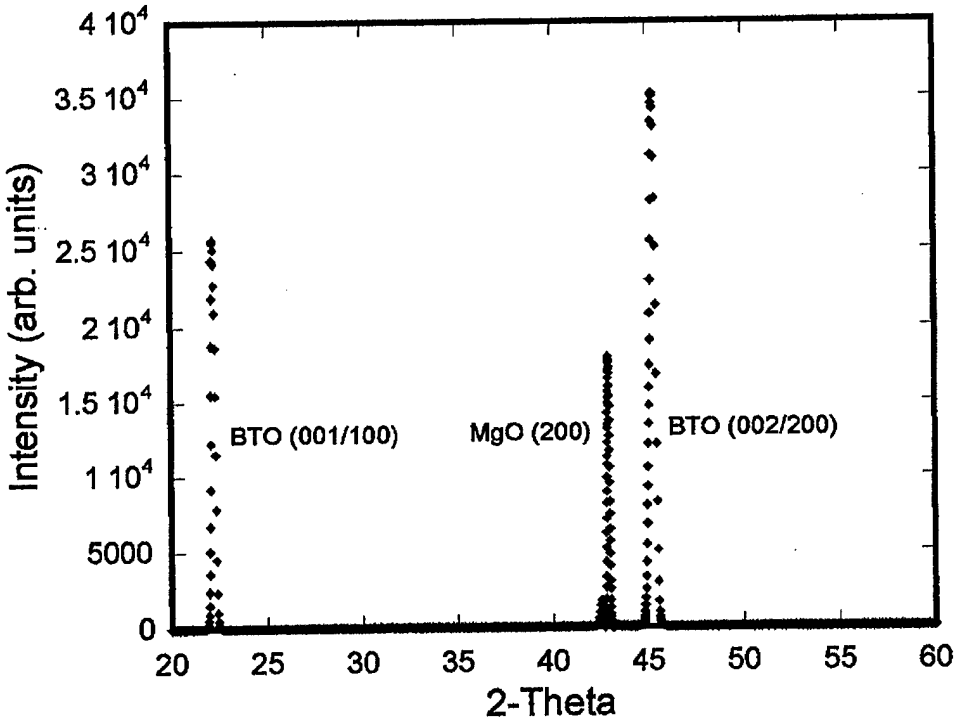


**Figure 1:** Theta-2theta x-ray diffraction scan of a Pr-doped $BaTiO_3$ thin film. The BTO is epitaxially oriented relative to the MgO substrate, and no impurity phases were observed.

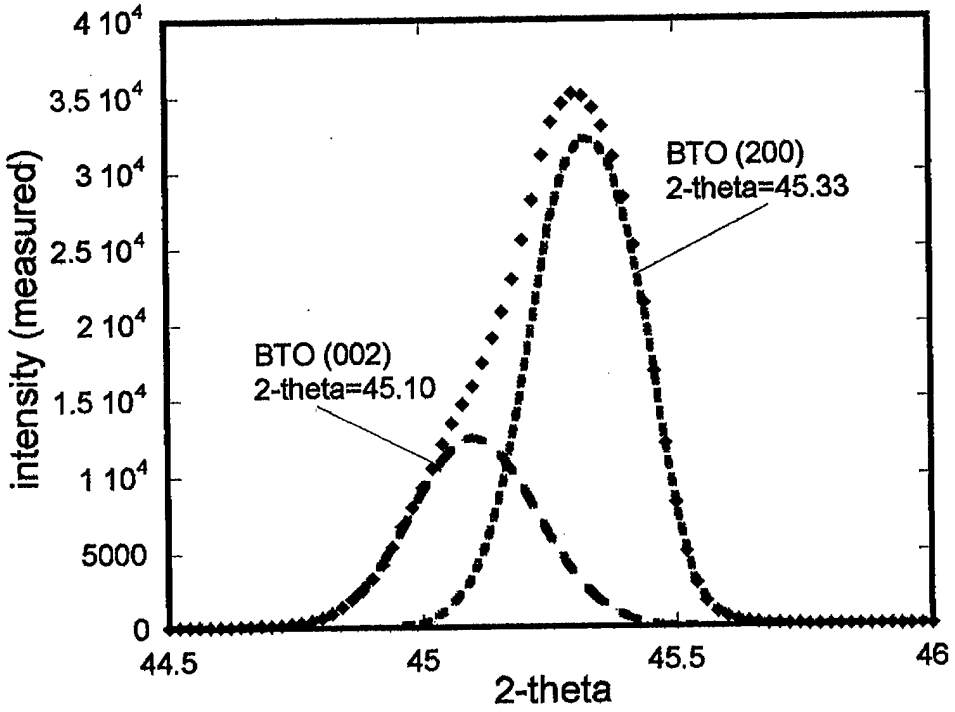


**Figure 2:** Close-up of the $BaTiO_3$ (002) and (200) peaks, showing the polydomain nature of the film.

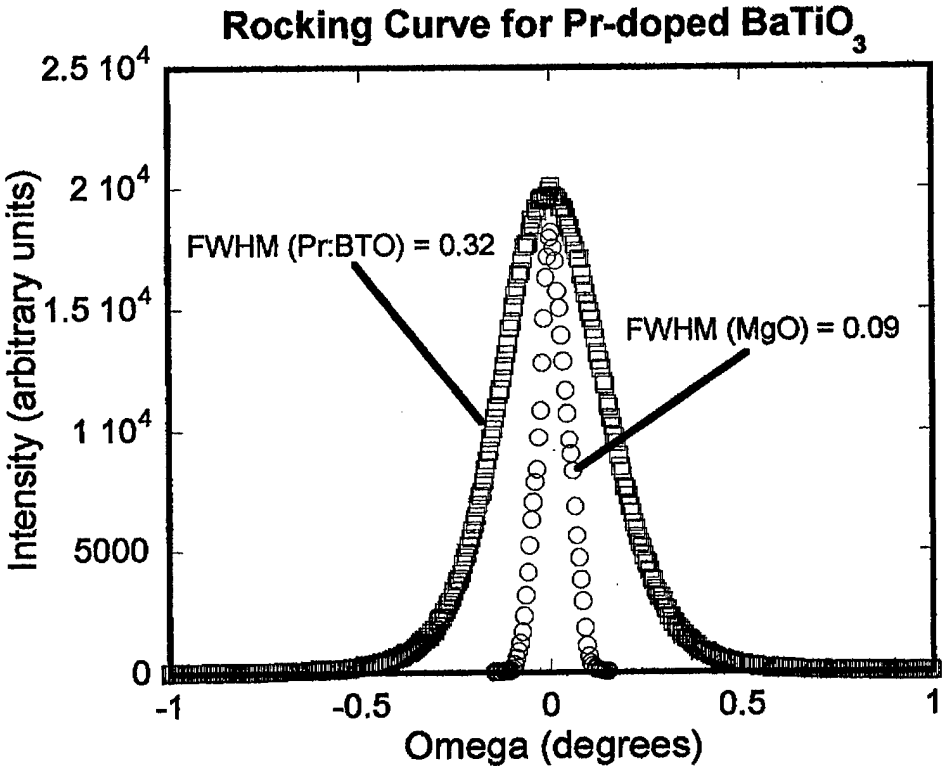


**Figure 3:** X-ray rocking curve for the (200) peaks of the Pr-doped BTO and the MgO substrate. The narrow full width at half maximum indicates a high state of crystalline perfection.

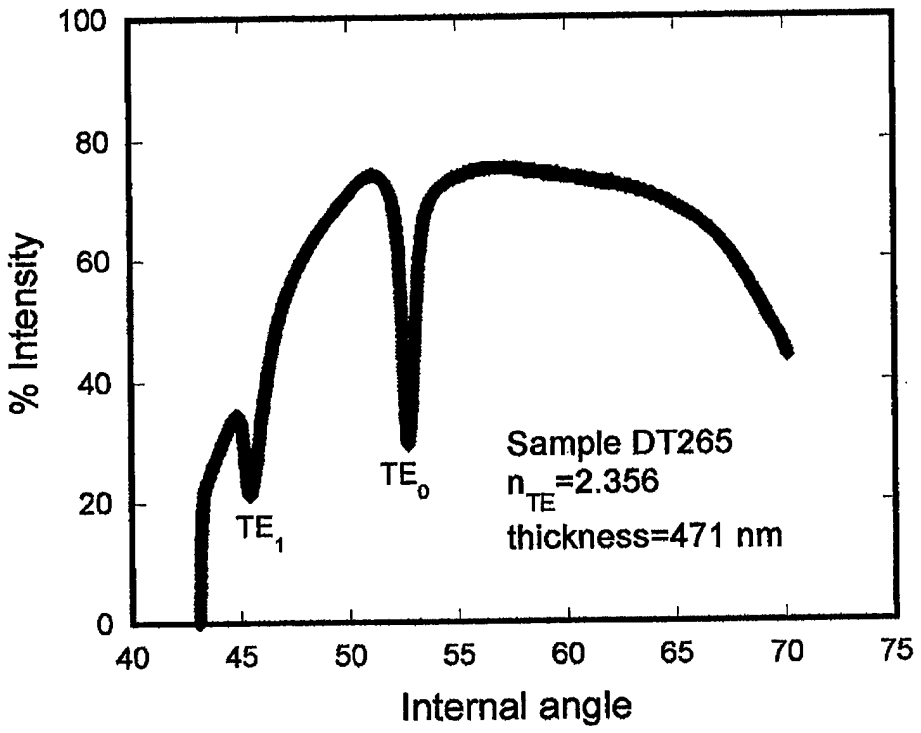


**Figure 4:** m-line spectroscopy spectrum of a Pr-doped $BaTiO_3$ film showing it supports two transverse electric (TE) optical modes at this wavelength ($\lambda$=632.8 nm).

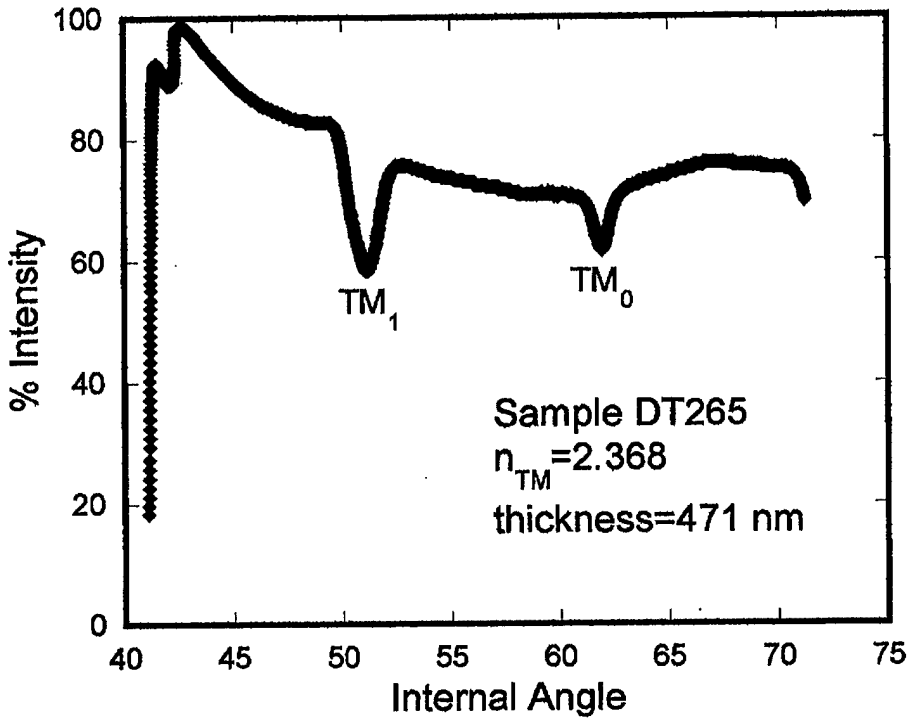


**Figure 5:** m-line spectroscopy of a Pr-doped $BaTiO_3$ using transverse magnetic (TM) polarization showing two guiding modes are supported.

The following page shows recent spectroscopic results, the inhomogeneously broadened absorption spectra for praseodymium in yttrium silicate at two crystalline sites. This represents work precursor to pursuing the spectroscopy in barium titanate. Dr. Renu Tripathi working in the laboratory of Selim Shahriar at Northwestern University performed this spectroscopy.

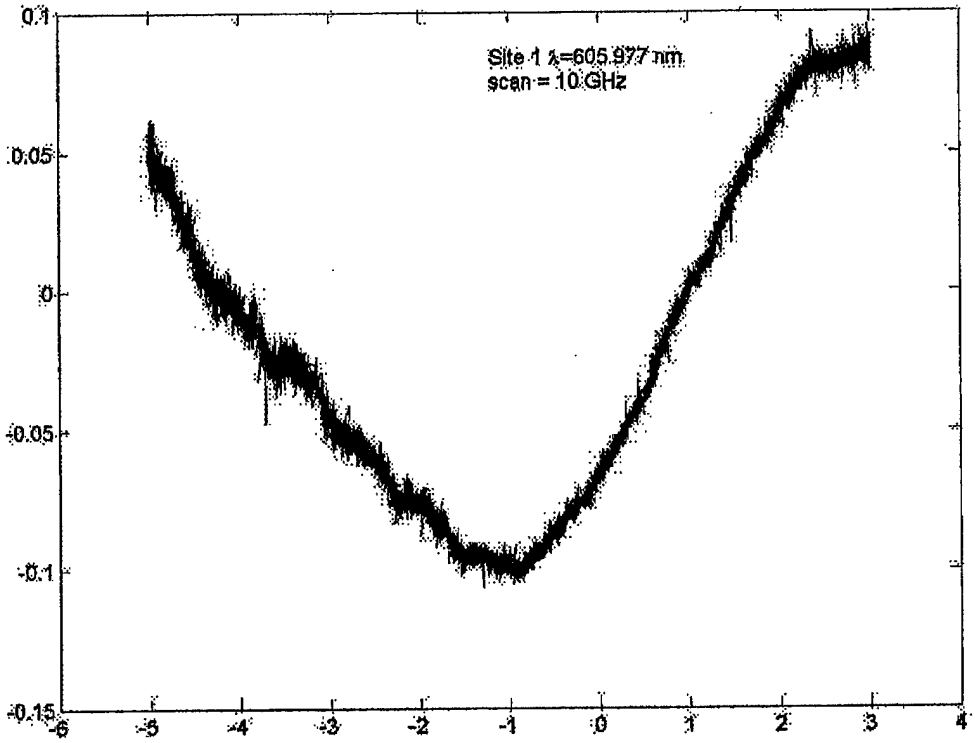
Site 1 λ=605.977 nm
scan = 10 GHz
0.1
0.05
0
-0.05
-0.1
-0.15
-6
-5
-4
-3
-2
-1
0
1
2
3
4

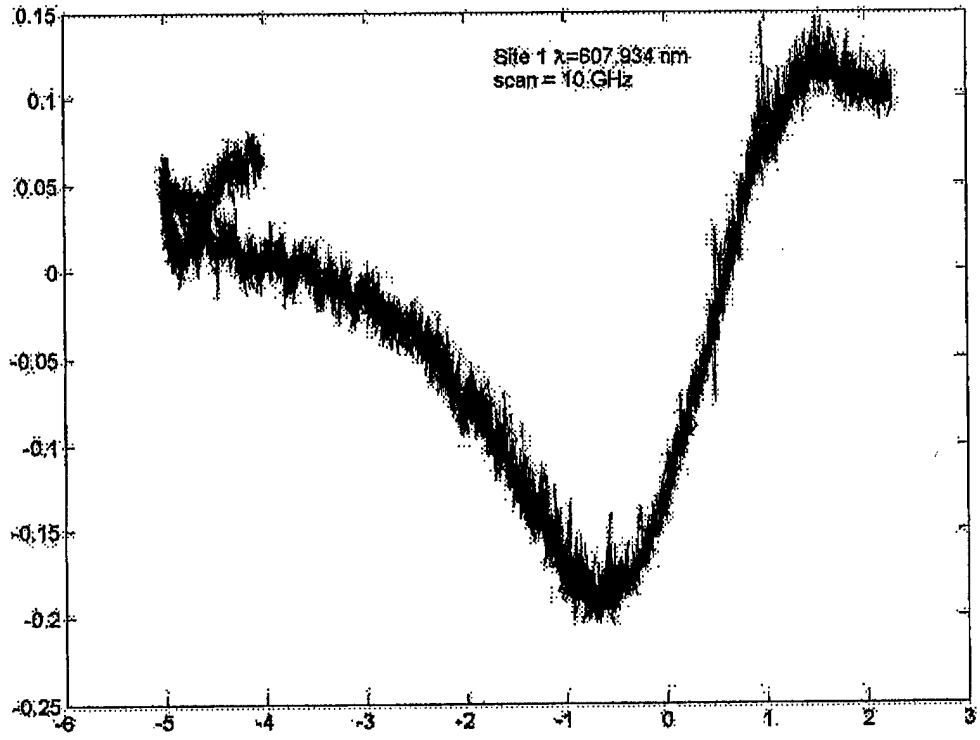
Site 1 λ=607.934 nm
scan = 10 GHz
0.15
0.1
0.05
0
-0.05
-0.1
-0.15
-0.2
-0.25
-6
-5
-4
-3
-2
-1
0
1
2
3

Nanophotonic Modulator using Electromagnetically Induced Transparency
Final Report References

1. Adiabatic population transfer in a three-level system driven by delayed laser pulses, J. R. Kuklinski et al., Phys. Rev. A, Vol 40, No. 11, p. 6741 (1989).
2. Observation of Ultraslow and Stored Light Pulses in a Solid, A.V. Turukhin, et al., Phys. Rev. Lett., Vol. 88, No. 2, p. 023602-1 (2002).
3. Integrated Optics, T. Tamir, ed., Springer Verlag, (1975).